COMPUTING AND ALGORITHM INSIGHT
Volume 1, Issue 1, June 2023 | pp. 71-98
https://doi.org/00.0000.000/xxxxx

OPEN ACCESS
Check for updates

SECURE IOT-BASED SMART HEALTHCARE: INTEGRATING BLOCKCHAIN AND DEEP LEARNING FOR AUTONOMOUS CLINICS AND PHARMACEUTICAL MANAGEMENT

Putra Pratama[1] ✉, Siti Rahayu[1], and Agus Wijaya[2]

Department of Computer Science, Universitas Muria Kudus, Kudus, Central Java, Indonesia[1]; Faculty of Engineering, Universitas Wiralodra, Indramayu, West Java, Indonesia[2]

ABSTRACT

The Internet of Things (IoT) has revolutionized smart healthcare, proving indispensable during the COVID-19 pandemic. However, the resource-constrained nature of IoT devices often precludes robust encryption, rendering systems vulnerable to privacy breaches and cyberattacks that threaten medical data integrity. To mitigate these risks, this study explores the synergy between IoT and blockchain technology to bolster security and transparency. Building on existing research, this paper outlines three key contributions: (1) an architecture for an autonomous, unsupervised medical clinic designed to deliver rapid care while minimizing infection exposure for staff; (2) a deep learning diagnostic model utilizing ResNet152 transfer learning for automated COVID-19 detection from X-ray images; and (3) a secure blockchain-enabled pharmaceutical distribution system. Experimental validation confirms that the proposed frameworks demonstrate the necessary efficacy, security, and robustness for reliable deployment in clinical environments.

Keywords: *Internet of Things (IoT); Blockchain Technology; Smart Healthcare; Deep Learning; COVID-19 Detection.*

CORRESPONDING AUTHOR:
Putra Pratama
Department of Computer Science, Universitas Muria Kudus, Kudus, Central Java, Indonesia
contact: *putra.pratama@umk.ac.id*

ARTICLE HISTORY
Received : April 20, 2023
Final Revised : May 31, 2023
Accepted : June 19, 2023
Published : June 30, 2023

© 2023 The Author(s) | Published by Integra Academic Press | This article is an open access article and distributed under the terms and conditions of the Creative Commons Attribution (CC BY-SA) license.

1. | INTRODUCTION

The emergence of COVID-19 and its subsequent variants has placed unprecedented strain on the global health sector. Health systems worldwide face the complex challenge of balancing the intensified demand for pandemic management services while simultaneously sustaining and enhancing access to essential medical care [1].

Health and Care Workers (HCWs) are central to the global response to the pandemic. They encounter heightened occupational risks due to exposure to this rapidly transmitting virus, necessitating significant adaptations in their professional roles and responsibilities [2]. The healthcare sector remains one of the most severely impacted industries, with personnel facing numerous hazards that compromise their physical, mental, and social well-being. Notably, HCWs exhibit a higher susceptibility to COVID-19 infection compared to the general population [3].

The pandemic has resulted in significant morbidity and mortality among HCWs and their families. Currently, the extent of these consequences is being assessed using a combination of anecdotal evidence and evaluation criteria of varying quality [2].

Furthermore, the crisis has adversely affected workforce availability and the capacity to deliver critical services amidst expanding demand. Throughout the COVID-19 pandemic, medical personnel have contended with shortages of Personal Protective Equipment (PPE) and essential supplies, infection risks, quarantine mandates, social stigma, physical assaults, and the dual burden of caring for their own families [3]. Consequently, there is an urgent need for innovative solutions to protect healthcare professionals. To address this, this study proposes an automated smart health system that operates without direct medical staff intervention, utilizing COVID-19 as a primary case study.

Approaches for estimating COVID-19-associated mortality among HCWs have been categorized into several algorithmic methodologies [3]:

1. Crude Mortality Rate Approach: The first method estimates HCW deaths by utilizing crude mortality rates from national data or the total fatalities reported to the World Health Organization (WHO) divided by population size. This model assumes that HCWs share similar infection and mortality risks with the general populace, regardless of demographics, yet acknowledges a higher exposure risk (both occupational and community-based, particularly in regions lacking robust infection control). A major limitation of this approach is significant underestimation; for instance, only 6,643 HCW deaths were identified out of 3.45 million reported COVID-19 fatalities, as illustrated in Figure 1a.
2. Standardized Mortality Approach: The second method improves upon the first by employing age- and sex-indirect standardization. Reported COVID-19 fatalities were redistributed based on demographic mortality patterns reported to the WHO. Additionally, the International Labor Organization's (ILO) workforce estimates were adjusted against the 25–64 age demographic. This model suggests approximately 115,500 HCW fatalities (ranging from 80,000 to over 1.6 million) among the global workforce. When accounting for high-burden nations, estimates could surpass 180,000. However, this strategy assumes HCW exposure risks are equivalent to the general population, potentially ignoring specific occupational hazards, as depicted in Figure 1b.

3. Infection Analysis Approach: The third approach analyzes SARS-CoV-2 infection data, noting that HCWs comprised 12.5% (95% CI: 6.2%–23.5%) of total infections between March and July 2020. A declining trend in HCW infections supports a lower bound estimate of 6.2% (dropping from 5.7% in May 2020 to 1.8% by May 2021). By multiplying the prevalence of death among HCWs by the estimated infection rate, this method derives an estimate representing 6.2% of all nationally reported SARS-CoV-2 infections, as shown in Figure 1c.
4. Meta-Analysis Approach: The fourth method employs meta-analysis summary statistics, yielding a global estimate of 79,700 HCW fatalities (as presented in Figure 1d), which aligns with an 83,000 figure (within a range of 39,900 to 159,500). The lower bound of 39,900 is considered the least plausible scenario as it conflates the lowest infection rate (6.2%) with the lowest mortality rate (0.4%).

Ultimately, evidence suggests that the actual toll of COVID-19-related deaths among HCWs is significantly higher than official records indicate.

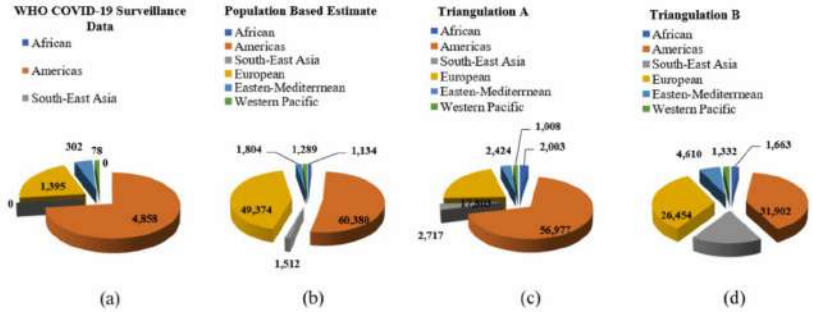


Figure 1. Comparative estimates of COVID-19-related mortality among Healthcare Workers (HCWs) between January 2020 and May 2021, derived via distinct methodological approaches. (a) Mortality data directly reported to WHO COVID-19 Surveillance; (b) Projections based on population demographics; (c) Estimates utilizing the indirect standardization technique; (d) Mortality figures derived from PCR-based meta-analysis.

Coinciding with the conclusion of the WHO's research, the Institute for Health Metrics and Evaluation (IHME) released findings derived from excess all-cause mortality methodologies [3]. Table 1 provides a comparative analysis of population-based estimates for COVID-19-related HCW fatalities within the top 20 countries—which collectively account for 80% of global deaths reported to the WHO—utilizing IHME's total mortality estimates as the denominator. Notably, considering the high-burden nations analyzed, the projected mortality among healthcare workers is anticipated to reach 179,500.

These statistics highlight an urgent imperative to implement robust protective measures for medical staff and their families, particularly given their pivotal role in navigating health crises and epidemics while sustaining routine care. Addressing this need, the present study proposes the development of an autonomous smart clinic capable of operating without direct human intervention. This system is designed to identify potential viral carriers and diagnose infected patients through a multi-stage process integrating temperature sensors, blood oxygen saturation levels, and X-ray imaging.

Table 1. Population-based estimates of HCW deaths: A comparison of WHO and IHME data for top-ranking countries (January 2020–May 2021) [3].

Country (Rank WHO / IHME)	Total COVID Deaths (% Share)	WHO HCW Deaths	Pop-Based Est. HCW Deaths	Indirect Standardization Est. (Total [Male / Female])	Meta-Analysis Est. Range (0.8% – 1.6%)	IHME Est. HCW Deaths
USA (1 / 1)	578,984 (17.3%)	593	99,925	37,633 [21,950 / 15,683]	16,137 – 32,274	62,426
Brazil (2 / 4)	430,417 (12.8%)	684	9,769	8,966 [5,430 / 3,536]	7,655 – 15,311	13,525
India (3 / 2)	266,207 (7.9%)	112	9,205	3,137 [867 / 5]	12,089 – 24,178	2,775
Mexico (4 / 3)	219,901 (6.6%)	3,214	2,717	2,870 [1,899 / 971]	1,178 – 2,356	7,625
UK (5 / 6)	127,668 (3.8%)	856	2,317	7,158 [6,151 / 922]	10,644 – 11	14,061
Italy (6 / 7)	123,927 (3.7%)	369	3,970	1,462 [810 / 652]	2,057 – 4,114	5,633
Russia (7 / 5)	115,480 (3.4%)	438	6,153	2,803 [729 / 2,446]	4,892 – 2	22,546
France (8 / 14)	106,666 (3.2%)	46	7,082	5,451 [2,821 / 2,632]	8,545 – 708	8,344
Germany (9 / 16)	86,025 (2.6%)	580	9,211	2,105 [610 / 561]	7,783 – 5,568	152
Colombia (10 / -)	79,760 (2.4%)	160	915	689 [161 / 515]	2,230 – 43	-
Spain (11 / 15)	79,095 (2.4%)	148	2,845	9,985 [034 / 9,951]	7,783 – 5,564	453
Iran (12 / 8)	76,433 (2.3%)	073	787	763 [923 / 813]	552 – 7,101	6,79
Poland (13 / 11)	71,609 (2.1%)	520	1,367	6,318 [358 / 1,415]	2,829 – 4,213	-
Argentina (14 / -)	69,254 (2.1%)	534	1,814	1,883 [1,209 / 674]	1,608 – 3	216
Peru (15 / 12)	65,316 (1.9%)	089	6,877	5,503 [2,792 / 918]	5,820 – 27	-
South Africa (16 / 10)	55,124 (1.6%)	096	6,162	905 [715 / 798]	1,596 – 2,812	-
Ukraine (17 / 13)	47,942 (1.4%)	615	1,342	4,482 [2,921 / 910]	672 – 1,333	877
Indonesia (18 / 17)	47,823 (1.4%)	031	4,534	3,212 [1,386 / 0]	1,720 – 7,60	-
Turkey (19 / -)	44,301 (1.3%)	0	8,033	1,817 [814 / 1,025]	2,750 – 5,500	-
Czech Republic (20 / -)	29,712 (0.9%)	87	110	3,367 [1,771 / 908]	1,616 – 32	-
Romania (21 / 19)	29,413 (0.9%)	126	5,221	4,100 [1,145 / 3,110]	6,219 – 43	-
Egypt (34 / 9)	14,206 (0.4%)	181	1,291	771 [2,156 / 1,212]	411 – 544	-
Japan (39 / 18)	11,365 (0.3%)	0	9,427	4,538 [935 / 6,333]	6,668 – 978	-
Kazakhstan (59 / 20)	4,760 (0.1%)	011	946	242 [220 / 340]	620 – 42	-
Sub-total			99,259	73,636 [42,748 / 30,888]	64,263 – 128,523	179,415

The rest of this paper is organized as follows: Section 2 provides a foundational overview of the Internet of Things (IoT) and blockchain technology. The architecture of the proposed autonomous smart clinic is detailed in Section 3. Section 4 delineates the deep learning methodology employed for COVID-19 detection utilizing X-ray imagery. The experimental results are rigorously analyzed in Section 5. Subsequently, Section 6 introduces the novel blockchain-based framework for pharmaceutical management. A comprehensive discussion of the findings is provided in Section 7. Finally, the paper concludes with a summary of contributions, acknowledgments, and a list of references.

2. | RELEVANT LITERATURE

This section provides a foundational overview of the Internet of Things (IoT) and blockchain technology, emphasizing their critical relevance to the healthcare sector. Furthermore, it reviews prior research exploring the integration of IoT and blockchain within medical ecosystems.

2.1. Internet of Things (IoT)

The Internet of Things (IoT) has permeated virtually every facet of modern society, driving innovation across diverse industries including automotive, energy, industrial manufacturing, and healthcare [4]. The healthcare domain, being inherently information-intensive, generates, collects, and transmits vast quantities of data. Managing the storage and dissemination of this data presents significant challenges due to strict security requirements and the highly sensitive nature of patient information.

Smart medical devices require specialized protocols for data processing and storage. Contemporary approaches often streamline the management of sensitive medical information and Electronic Health Records (EHRs) by outsourcing them to cloud-based storage solutions [5]. Compared to traditional on-premise systems, cloud-based medical infrastructures enhance diagnostic accuracy and reduce operational costs by facilitating information exchange, knowledge management, and predictive analytics across the healthcare ecosystem [6,7]. However, cloud computing introduces inherent vulnerabilities regarding data integrity, security, and potential data loss. A critical concern is the centralized administration of cloud environments, where a single authority manages access and may potentially share user health data with third parties for commercial purposes [8,9]. Consequently, there is a pressing need for secure mechanisms to handle patient medical information. Blockchain technology emerges as an optimal solution to these challenges by providing a robust, decentralized distributed ledger [10].

The EHR market is substantial, with valuations estimated in the tens of billions of dollars [11]. Nevertheless, the exchange of health data necessitates a secure and reliable infrastructure to mitigate risks associated with privacy, security, and interoperability. Firstly, health data requires stringent privacy protections, a concern that intensifies as reliance on cloud storage grows, increasing the potential for data leaks and unauthorized disclosure. Secondly, modern systems typically employ centralized architectures and security protocols, which complicates the interoperability of healthcare systems distributed across various locations. Furthermore, a significant limitation of current systems is the restricted access consumers have to their own private health data [12]. Given the increasing prevalence of mobile platforms and portable computing devices, alongside the growing emphasis on data self-ownership, it is imperative to

design next-generation EHR systems. These systems must ensure user access control and security in a manner that is both distributed and efficient [13].

Such advanced systems must be capable of secure and efficient data communication [14,15,16] while affording individuals greater control over access, privacy, and anonymity. Failure to adequately address security, privacy, and trust may lead to individuals withholding critical information or delaying necessary treatment [17]. Many existing health data systems rely on a single entity for data maintenance, creating a single point of failure. Blockchain technology, due to its decentralized nature, has the potential to eliminate this dependency, offering the capacity to distribute data immutably and resist both systemic failures and malicious attacks [13].

Additionally, blockchain serves as a verifiable record of data ownership and authenticity [13,18]. It enables the application of pseudo-anonymity combined with Public Key Infrastructure (PKI) to preserve user privacy [17]. The literature extensively discusses the application of blockchain in healthcare [19], supporting its utility for privacy-preserving predictive modeling, enhancing large-scale institutional interoperability, ensuring the immutability of health records, improving health assurance processes, facilitating data exchange, supporting AI-driven healthcare models, and managing identity and revenue cycles [19,20].

2.2. Introduction to Blockchain

A blockchain network enables the sharing of resources among users without the vulnerabilities associated with a single point of failure [21], effectively eliminating bottlenecks inherent to centralized systems. In this architecture, user data and links to the ledger are encapsulated within "blocks." A block permanently records the history of past transactions, while new transactions are appended to the current block. The protocol for adding a new block is governed by consensus mechanisms within the network [10].

Blockchain technology has been the subject of extensive investigation in recent years. Conceptually, it originated as the underlying mechanism for the digital cryptocurrency, Bitcoin [22]. The fundamental premise of blockchain is to facilitate cooperation between unacquainted and untrusted entities—validating the distributed nature of smart health devices—without requiring a central authority for security and authentication, a distinct departure from current cloud computing architectures [23]. This technology relies on an immutable "public ledger," a shared database accessible to all participants. This ledger consists of data blocks linked via cryptographic hash keys, a connecting process often secured through Proof of Work (PoW) [18]. By design, both the ledger and the consensus mechanism are tamper-resistant; once recorded, block data cannot be retroactively altered without invalidating subsequent block hashes and disrupting network consensus. This architecture allows Bitcoin's public distributed ledgers to execute digital financial transactions securely and cost-effectively without third-party validation, thereby resolving the "double spending" problem [23]. When a transaction is initiated, a smart contract may execute as a stored procedure. Key characteristics of blockchain technology include decentralized control, transparency, auditability, distributed information, and resilience against malicious actors [18,23].

Essentially, a blockchain is a distributed database of records derived from digital transactions executed by network participants [18]. Every transaction is authenticated by a majority of the network members and subsequently stored. Bitcoin represents one of the most robust applications of this technology, utilizing a network-distributed digital ledger to record

all transactions. As the name suggests, a blockchain is a sequence of interconnected blocks [18]. The addition of a single block involves four distinct steps. First, a transaction must occur; for example, a purchase made on an e-commerce platform like Amazon [13].

Second, the transaction must be validated. Similar to how public repositories like Wikipedia employ quality control for new entries, the blockchain utilizes a global network of computers to verify the transaction details, such as timestamp and amount. Third, the validated transaction is stored in a block. Once verified, the transaction is approved, and the block retains all relevant data, including monetary value and digital signatures. This block is then grouped with thousands of others [13].

Finally, a unique hash value is assigned to the new block. Upon validation, the block is secured with this identifiable hash and appended to the blockchain. Once added, the block becomes publicly visible, allowing users to verify when, where, and by whom the block was uploaded [13].

In summary, a blockchain is a chronological succession of blocks representing complete and valid transaction records. Each block is cryptographically linked to its predecessor via a hash value, forming a chain. The initial block in this sequence is termed the "genesis block," while the preceding block for any given block is referred to as the parent block. As illustrated in Figure 2, a block consists of two primary components: the block header and the block body [22].

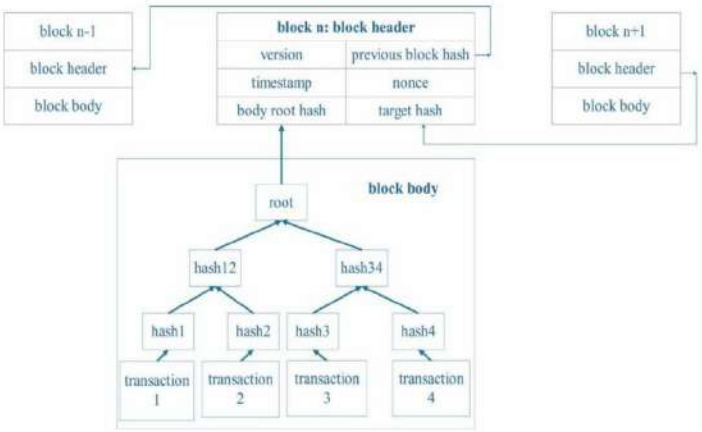


Figure 2. Block structure [22].

Here is the paraphrased version of the text, maintaining an academic tone and ensuring all citations and figure references are preserved.

The blockchain header encapsulates essential metadata [22]:

1. Block Version: Specifies the protocol validation rules.
2. Previous Block Hash: Links to the immediately preceding block.
3. Timestamp: Records the precise time of block creation.
4. Nonce: A 4-byte arbitrary field modified by miners during the Proof of Work (PoW) computation.
5. Body Root Hash: The Merkle tree root hash derived from the transactions contained within the block body.
6. Target Hash: The difficulty threshold required for a new block to be considered valid within the PoW mechanism.

The block body acts as the repository for verified transactions accumulated over a specific period. These transactions are organized using a Merkle tree structure, where leaf nodes represent individual transactions and non-leaf nodes consist of the concatenated hashes of their children. This hierarchical arrangement enables efficient verification of transaction existence and integrity; a node need only validate the hash path of relevant branches rather than the entire tree. Any alteration to a transaction propagates upward, invalidating the root hash [24]. The capacity of a block is constrained by both the block size limit and individual transaction sizes. Blocks are sequentially linked via cryptographic hashes in an append-only format. Due to the computational infeasibility of altering previously validated data without invalidating subsequent blocks, the system achieves robust immutability and security [25].

Blockchain architectures are generally categorized into three types [26,27]:

1. Public (Permissionless): Open networks where any participant can execute transactions, mine blocks, or operate a node (e.g., Bitcoin).
2. Private (Permissioned): Restricted networks accessible only to authorized members of a specific organization.
3. Consortium: Hybrid systems governed by a group of organizations rather than a single entity, balancing centralization and decentralization.

The primary advantages of blockchain implementation include [27]:

1. Time Efficiency: Bypassing central authority validation accelerates settlement processes.
2. Cost Reduction: Direct peer-to-peer asset transfer eliminates intermediaries and associated overheads.
3. Enhanced Security: The distributed nature of the ledger makes data tampering computationally impractical, thereby deterring fraud and cybercrime.

Blockchain technology offers significant benefits for establishing trust and efficiency within the healthcare ecosystem:

1. Patient Consent Administration: The integrity of Electronic Health Records (EHRs)—comprising diagnoses, treatments, and medical history—is critical for effective virtual care [28]. Blockchain facilitates the secure sharing of sensitive data among stakeholders (hospitals, pharmacies, regulators) without intermediaries. It enforces data access rules, thereby empowering patients with greater control and ownership over their clinical information in compliance with telemedicine regulations [29,30].
2. Remote Treatment Traceability: Telehealth relies on seamless electronic and face-to-face interactions between patients and specialists via Direct-to-Consumer (D2C) and Business-to-Business (B2B) models. Traditional systems often trap patient data in silos, hindering comprehensive care [31]. Blockchain unifies these fragmented records, providing a consistent, auditable view of a patient's history. This transparency allows for rigorous auditing of data access and transaction history [30,31,32].
3. Traceability of In-Home Medical Kits: Self-diagnostic kits facilitate early disease detection and cost reduction. However, centralized systems often lack transparency regarding the provenance of these devices. Blockchain provides an immutable ledger to track the ownership, performance, and authenticity of medical kits, ensuring patients and physicians utilize reliable products [32].
4. Security of Personal Health Records (PHR): Unlike EHRs, PHRs are managed by the data owner. Storing PHRs on centralized cloud platforms introduces risks of single-

point failure and data integrity compromise. Blockchain's decentralized architecture ensures that medical data remains private and secure under the owner's control [29,31,33].

5. Automated Payments: Blockchain facilitates micropayments using cryptocurrency tokens, creating a fast, transparent, and auditable payment infrastructure. This eliminates the need for central clearinghouses and mitigates payment disputes between patients and service providers [28,34].
6. Reliable Elderly Care Monitoring: IoT-enabled biomedical sensors allow for continuous remote monitoring of vital signs [26]. To prevent medical errors arising from faulty device data, blockchain smart contracts verify the identity and access rights of these sensors before recording data to the ledger [31]. Additionally, these systems can trigger automated alerts to medical centers during emergencies or manage medication refills proactively [35].
7. Drug Delivery and Pharmacy Traceability: Hash functions within the blockchain verify prescription integrity, reducing errors and preventing unauthorized alterations [28,36]. Pharmacists can authenticate prescriptions, while patients can track the shipment of medications. This end-to-end traceability confirms the legitimacy and provenance of pharmaceutical products [31].
8. Trustworthy Health Insurance Services: Blockchain mitigates insurance fraud by providing a verified, consent-based access mechanism to medical records [28,33,34]. Furthermore, insurers can incentivize healthy behaviors (e.g., gym attendance verified by smart devices) through cryptocurrency rewards, fostering a trust-based relationship with policyholders.
9. Reputation-Based Specialist Referrals: Referral documents can be stored on IPFS servers with their corresponding hashes recorded on the blockchain, ensuring data integrity and accessibility for consulting specialists [31]. Following consultation, specialists can upload diagnosis reports, and referring providers can update reputation scores based on service quality and patient satisfaction [31].
10. Automated Patient Follow-Up: Smart contracts streamline follow-up care by automatically notifying patients and staff of upcoming appointments. Physicians can access immutable EHRs to review prior health status, while patients can securely share medical reports stored on IPFS servers via registered hashes [28,31,33].

3. | THE PROPOSED SMART CLINIC

This section delineates the design of the proposed autonomous smart medical clinic, which is engineered to perform patient diagnosis without the direct intervention of medical staff. The operational model is designed for sequential processing, ensuring that the facility accommodates a single patient per session before resetting the workflow for subsequent admissions.

The proposed algorithmic framework is bifurcated into two distinct phases. The first phase constitutes the Digital Interface Component, accessible via the clinic's web portal, and proceeds through three sequential steps:

1. Patient Onboarding: This involves user registration, demographic data collection, and the logging of clinical symptoms.

2. Scheduling: The system generates a unique Quick Response (QR) code for authentication and determines an optimal appointment slot.
3. Preliminary Protocol: Based on the input data, the system suggests a tentative treatment protocol.

The second phase constitutes the Physical Consultation, which occurs on-site and comprises two critical diagnostic stages:

1. Biometric Sensing: The acquisition of vital physiological measurements.
2. Imaging: The execution of diagnostic X-ray procedures.

A schematic block diagram illustrating these operational phases is depicted in Figure 3.

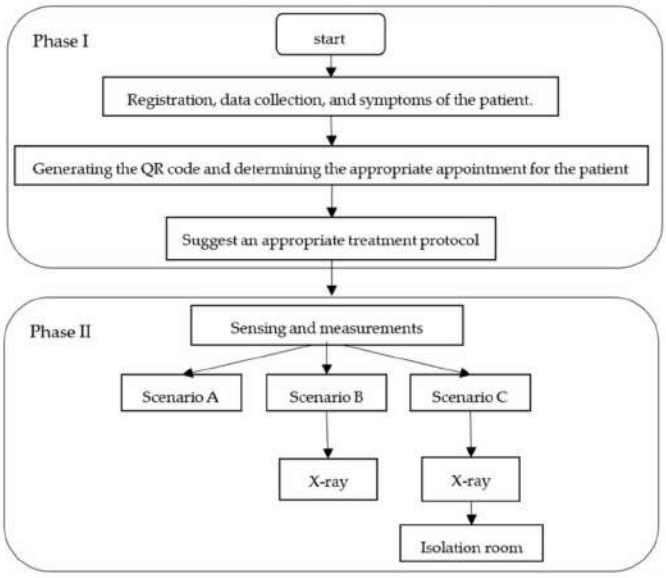


Figure 3. Schematic representation of the operational phases and workflow within the proposed smart clinic framework.

3.1. Phase I: The Clinic's Website

The clinic's website functions as a contactless digital interface, establishing a communication channel between patients and physicians that eliminates the need for physical interaction. Given the exponential surge in COVID-19 cases, healthcare providers and hospitals frequently face capacity constraints that limit their ability to treat large patient volumes simultaneously. Consequently, a primary objective of this platform is to systematically organize and schedule patient appointments to manage facility throughput. Furthermore, the system optimizes medical resource allocation, enabling a single practitioner to provide remote consultations and guidance to a broad patient demographic efficiently. The user interface of the clinic's landing page is illustrated in Figure 4.

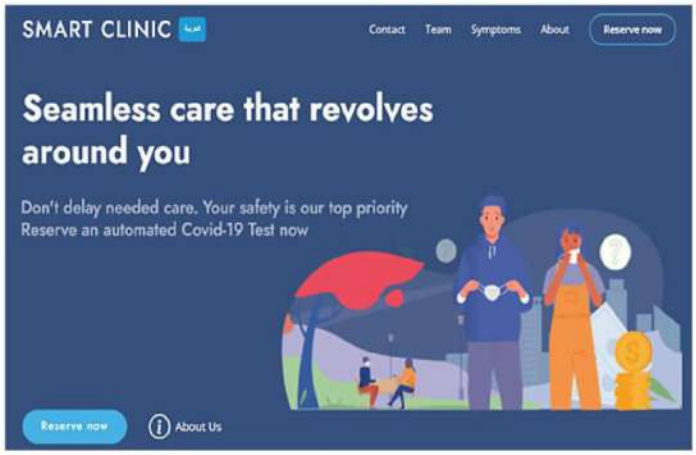


Figure 4. The front page interface of the proposed clinic website.

There are three steps offered by the website that the patient must take when they enter the website, including the following:

1. Registration, Data Collection, and Receiving Symptoms of The Patient

When a person feels tired, or some symptoms of COVID-19 are experienced, they can enter the clinic's website to register and fill out the form that includes two parts:

a. Data Collection

Personal information such as Name, National ID, gender, phone number, etc. The form is shown in Figure 5.

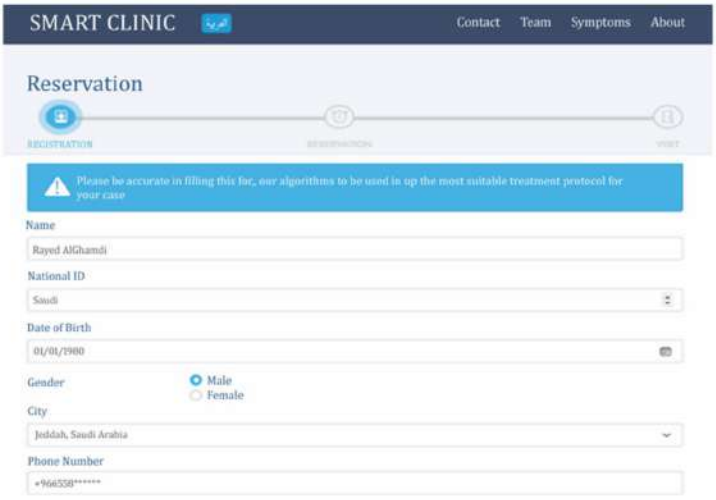


Figure 5. The registration form.

b. Patient Symptom and History Acquisition

The data collection process involves gathering comprehensive patient-specific medical information, which is categorized into three primary domains:

- Comorbidities: Information regarding pre-existing chronic conditions (e.g., diabetes, hypertension, cardiovascular diseases, obesity, malignancies, and asthma).

- Clinical Manifestations: Current symptoms experienced by the patient (e.g., pyrexia, cough, fatigue, anosmia or ageusia, pharyngitis, cephalgia, myalgia, gastrointestinal distress, and conjunctival irritation).
- Lifestyle Factors: Specifically, the patient's smoking status.

This cumulative dataset is utilized to determine the most appropriate therapeutic protocol for each individual.

2. QR Code Generation and Appointment Scheduling

Upon completing the medical questionnaire, the patient selects a preferred date and time for the on-site examination. Following the confirmation of the reservation via the "submit" function, the system generates a unique Quick Response (QR) code, as illustrated in Figure 6. This code serves as an authentication credential granting access to the clinic facility. Simultaneously, the patient's unique identifier (ID), appointment details, and the associated QR code are securely archived within the central database to facilitate verification upon arrival.

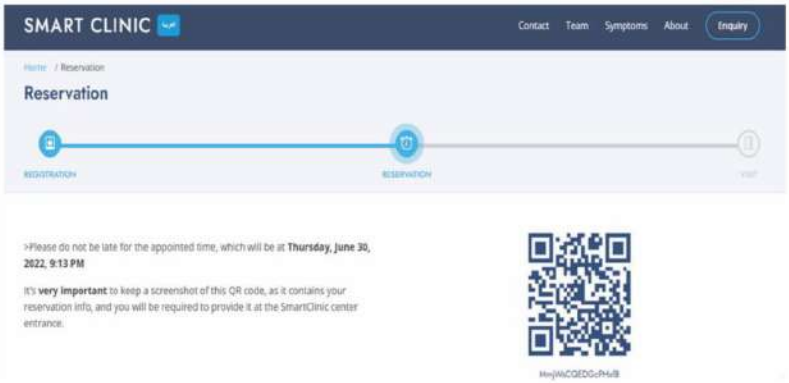


Figure 6. QR code generation.

3. Suggestion of an appropriate treatment protocol

Subsequent to the patient's on-site examination, an optimal therapeutic regimen is algorithmically proposed, contingent upon the derived diagnostic findings.

3.2. Phase II: Clinic Visit

Facility access is secured via a QR code authentication system located at the entrance, requiring the patient to scan their unique credential to gain entry. The clinic's operational architecture is organized into two fundamental diagnostic phases: the biometric sensing station and the X-ray imaging suite. The internal layout of this smart facility is depicted in Figure 7.

Procedural workflow is dynamically determined by the patient's real-time physiological parameters, specifically body temperature and blood oxygen saturation (SpO2). This triage logic results in distinct directional pathways:

1. Scenario I (Normal): Patients exhibiting normal vital signs are guided along the Green Path ("Path A").
2. Scenario II (Abnormal): Patients with irregular readings are diverted to either the Yellow Path ("Path B") or the Red Path ("Path C"), depending on the specific diagnostic criteria.

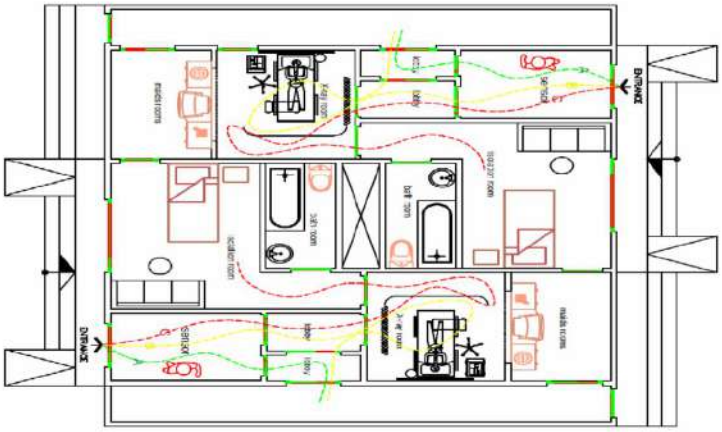


Figure 7. Schematic design of the proposed smart clinic structure.

This initial phase involves the acquisition of physiological parameters utilizing a suite of specialized sensors and measurement hardware. A schematic representation of the sensing and measurement architecture within the smart clinic system is illustrated in Figure 8.

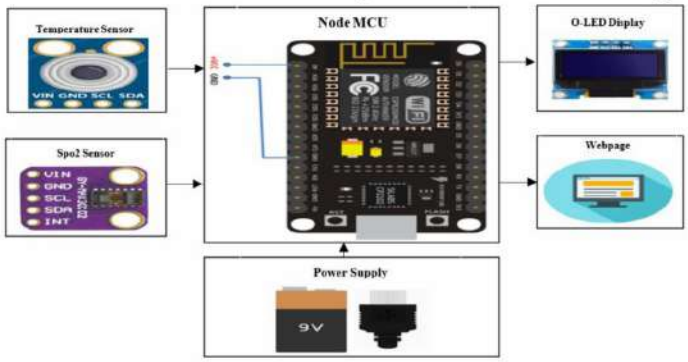


Figure 8. Schematic diagram of the sensing and measurements stage.

The hardware configuration for this stage comprises five integral components: the Node-MCU microcontroller, biometric sensing elements (specifically for SpO2 and Body Temperature), a power supply unit, an O-LED visual display interface, and a web-based connectivity layer.

The Node-MCU functions as the central processing unit of the system. It is a cost-effective, versatile IoT platform capable of establishing Wi-Fi connectivity to communicate with the broader Internet or generating its own ad-hoc network for direct device interfacing. Its ability to operate on a low-voltage power supply enhances its applicability in diverse settings. Functionally, the Node-MCU aggregates data from the thermal and blood oxygen sensors, visualizes the real-time readings on the O-LED screen, and manages the transmission of this data to the web server.

The proposed architecture integrates two primary diagnostic sensors: the MAX30100 for monitoring blood oxygen saturation (SpO2) and the MLX90614 for thermal screening.

1. SpO2 Level (MAX30100):
    - Blood oxygen saturation (SpO2) quantifies the ratio of oxygenated hemoglobin to deoxygenated hemoglobin, expressed as a percentage. Clinical standards indicate that a healthy human baseline should exceed 94%.

- The sensor employs pulse oximetry technology, leveraging the differential absorption of light; oxygenated hemoglobin absorbs infrared light, while deoxygenated hemoglobin absorbs red light. The sensor calculates SpO2 based on the transmission and absorption rates of these wavelengths.

Additionally, the sensor derives the Pulse Rate (PR) by analyzing variations in the volumetric pressure wave amplitude caused by the heartbeat. Standard adult heart rates typically fall within the 60 to 100 beats per minute (bpm) range. The structural design of the pulse oximeter is depicted in Figure 9.

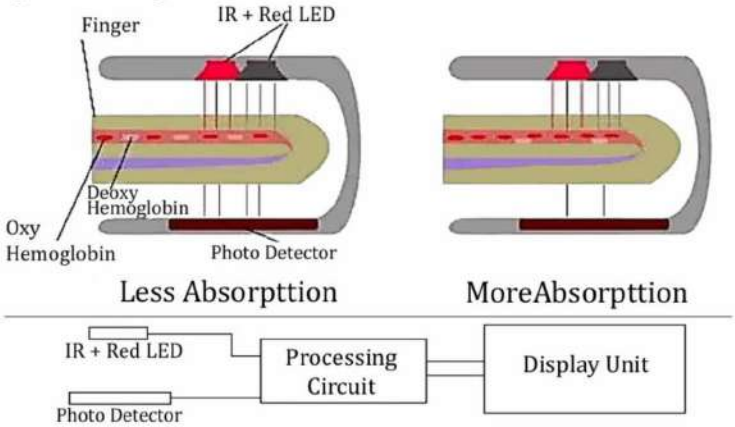


Figure 9. The structure of the pulse oximeter.

2. Temperature Sensor (MLX90614):
   - Thermal measurement is conducted using the MLX90614, a non-contact digital infrared (IR) sensor. It operates on the Stefan-Boltzmann principle, which correlates the IR radiation emitted by an object to its temperature. This sensor is capable of measuring temperatures ranging from −70 °C to 382.2 °C. It communicates with the microcontroller via the I2C protocol, enabling precise thermal screening without physical contact.

Thoracic X-ray imaging serves as a critical screening tool for identifying potential COVID-19 infection. These images frequently reveal pathological indicators, such as lung consolidation associated with viral pneumonia. The technical specifications of the deep learning model used in this step are detailed in Section 5.

The operational workflow branches into two distinct scenarios based on the physiological data (Temperature and SpO2) acquired in Stage 1:

Scenario I: The Non-Critical Pathway

1. A patient is classified as "Negative" for immediate COVID-19 risk if they exhibit either: (1) Normal temperature and normal SpO2, or (2) Elevated temperature with normal SpO2.
2. These patients are directed along the Green Path ("Path A") towards the lobby to exit via the side door (as shown in Figure 7). Following their departure, the area undergoes an automated sterilization process.
   - Sub-case 1: Patients with normal vitals are discharged home.
   - Sub-case 2: Patients with pyrexia (fever) but normal oxygen saturation are advised to proceed to standard medical service rooms to investigate the non-COVID etiology of the fever.

Scenario II: The Critical Pathway

1. A patient is flagged as a potential case if they exhibit both elevated temperature and abnormal (low) SpO2 readings. This combination significantly increases the probability of viral infection or carrier status, necessitating further diagnostic validation via X-ray.
2. The patient undergoes chest X-ray screening, which is analyzed by the ResNet152 deep learning model. The output is a binary classification: "Negative Case" or "Positive Case."
   - Negative Classification: The patient proceeds via the Yellow Path ("Path B") to the exit, followed by facility sterilization.
   - Positive Classification: The patient is routed via the Red Path ("Path C") to isolation units. Based on the diagnosis and registration data, a specific treatment protocol is assigned.
3. All diagnostic outcomes are archived in the central database to form the patient's medical history. For patients opting for home isolation, comprehensive care instructions and treatment protocols are provided via their personalized digital portal.

This section explains the steps the writer took in the research, and provides a brief justification for the method used. In this section the writer must present enough information to enable the reader to be able to evaluate the suitability of the method, the reliability and the validity of your findings. It would be better if the information presented could be replicated by other researchers in the future.

The methodology section usually has several sub-sections:

1. Sampling (description of target population, research context and unit of analysis; examples; and profile of respondents)
2. Data collection
3. Measures (Alternatively, Measurement)

4. | THE PROPOSED COVID-19 DETECTION FROM AN X-RAY IMAGE USING DEEP LEARNING

This section delineates the diagnostic methodology employed to ascertain the presence of COVID-19 pathology from the X-ray imagery acquired during Stage 2 (detailed in Section 3). The proposed algorithmic framework is founded upon a Convolutional Neural Network (CNN) architecture. Specifically, this study implements the ResNet152 model, leveraging transfer learning from a pre-trained state on comparable medical imaging datasets. The efficiency and suitability of this architecture for the target application are critically discussed. Subsequently, the development of the customized detection algorithm based on the ResNet152 backbone is elaborated. The functional block diagram illustrating the complete COVID-19 detection workflow is presented in Figure 10.

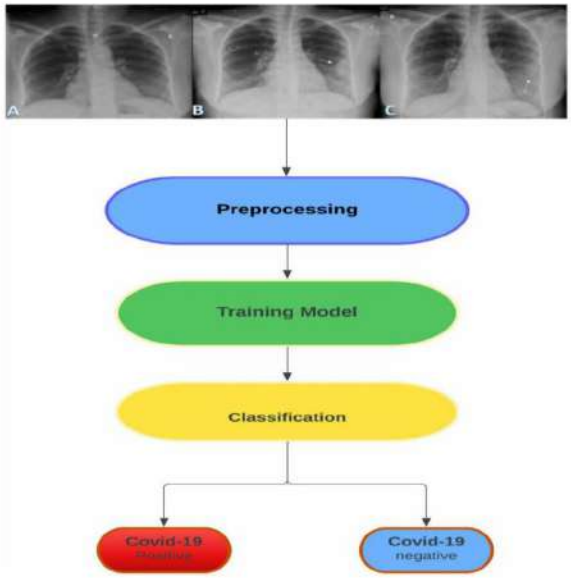


Figure 10. The operational block diagram for the X-ray detection algorithm, with (A–C) indicating sample input images.

The algorithmic framework, as illustrated in Figure 10, initiates with the aggregation of X-ray imagery from diverse heterogeneous datasets. Subsequently, a preprocessing phase is executed, employing various techniques to enhance and standardize the collected images. Following enhancement, the data is partitioned into distinct training and testing subsets. Ultimately, the classifier is evaluated using the unseen testing images to discriminate between positive and negative cases. Detailed delineations of these procedural stages are provided in Sections 4.1 through 4.4.

4.1. Dataset Construction

Given the dynamic nature of medical databases, the dataset utilized in this study was amalgamated from multiple continuously updated, open-access radiology repositories:

1. Radiopaedia [37]: An open-edit collaborative resource where radiologists contribute daily case studies.
2. SIRM [38]: The official database of the Italian Society of Medical and Interventional Radiology, which hosts a dedicated COVID-19 collection.
3. EuroRad [39]: A peer-reviewed repository of radiological case reports.

Following the aggregation and curation process, the final dataset distribution comprises 43% normal (healthy) images and 57% COVID-19 positive images.

4.2. Preprocessing

Post-acquisition, the raw imagery undergoes a rigorous preprocessing phase to ensure uniformity across the dataset. Initially, all images are rescaled to a standardized resolution of 224×224 pixels. To enhance model robustness and mitigate the risk of overfitting, a suite of data augmentation techniques is applied. These operations include resizing, shearing, zooming, rotation, padding, horizontal flipping, and cropping, thereby introducing variance to the training data.

4.3. Training Model

Once the images are standardized in terms of dimension and orientation, the dataset is stratified into training and testing subsets. An 80:20 split ratio is employed, wherein 80% of

the dataset is allocated for training the deep learning classifier, while the remaining 20% is reserved for independent validation. The training phase is executed over a duration of 20 epochs to optimize model convergence.

4.4. Classification

The core of the classification engine relies on a Residual Neural Network (ResNet), a specialized deep learning architecture derived from Artificial Neural Networks (ANN). ResNet operates as a gateless or open-gated variant of HighwayNet. The proposed model is optimized through the fine-tuning of specific hyperparameters.

The system utilizes transfer learning, a methodology that repurposes knowledge from a pre-trained base model to a new target task. This approach serves as an optimization strategy, significantly reducing computational expenditure and training time while enhancing efficiency. Transfer learning is particularly advantageous when feature sets possess universal applicability across source and target domains. Generally, this process involves either extracting fixed features from intermediate layers or fine-tuning the model weights with new data samples.

In this study, the ResNet152 architecture is employed. The model retains the pre-trained network weights, while the final fully connected layer is replaced to suit the specific binary classification task. Figure 11 depicts the ResNet architecture processing an input x. The network learns the residual mapping, defined as $F(x) - x$, relative to the essential mapping $F(x)$, prior to the application of the activation function at the block's output.

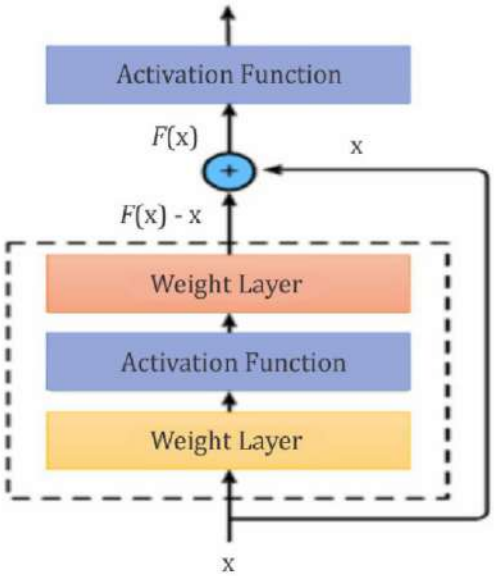


Figure 11. ResNet architecture.

A Residual Neural Network (ResNet) is made up of an input layer, four stages, and an output layer, as shown in Figure 12. Each stage indicates a step in the process that is carried out sequentially. It takes input from previous stages, runs one step of the CNN, and outputs the results. ResNet is broken into five stages, with Stage 0 serving as a pre-processing of input and the latter four stages consisting of a bottleneck and having a more comparable structure. In addition, an input stem performs a 7-7 convolution, has 64 output channels, and a stride of 2. Following that is a 3-3 max pooling layer with a stride of 2. The input width and height were effectively reduced four times in this layer, but the channel size was increased to 64.

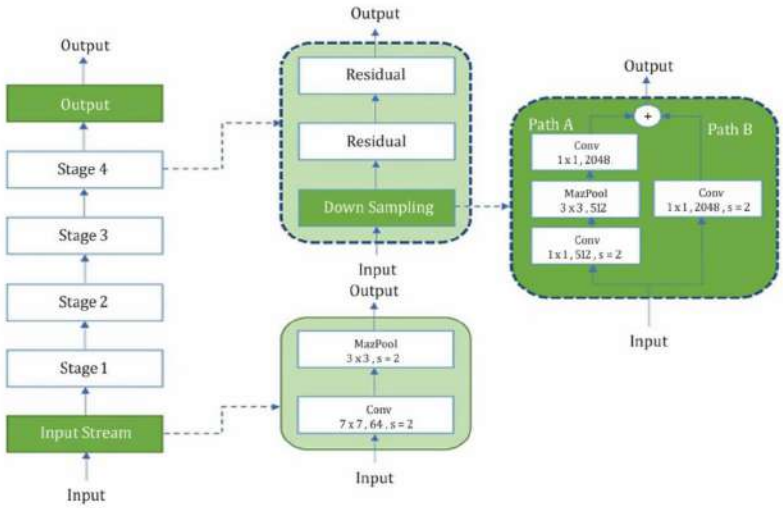


Figure 12. ResNet structural overview showing convolution kernels and pooling layer dimensions.

The architecture incorporates down-sampling blocks alongside residual blocks throughout Stage 2 and subsequent phases. Functionally, residual blocks mirror the operation of down-sampling blocks, with the primary distinction being the convolutional stride configuration, which is set to 1 in this context. Modulating the quantity of these residual blocks generates distinct model variants, such as ResNet50 and ResNet152, wherein the numerical suffix explicitly denotes the total depth of convolutional layers within the network. The fundamental constituents of the ResNet architecture encompass convolutional layers, activation units, pooling mechanisms, and batch normalization protocols. These essential components are schematically illustrated in Figure 13.

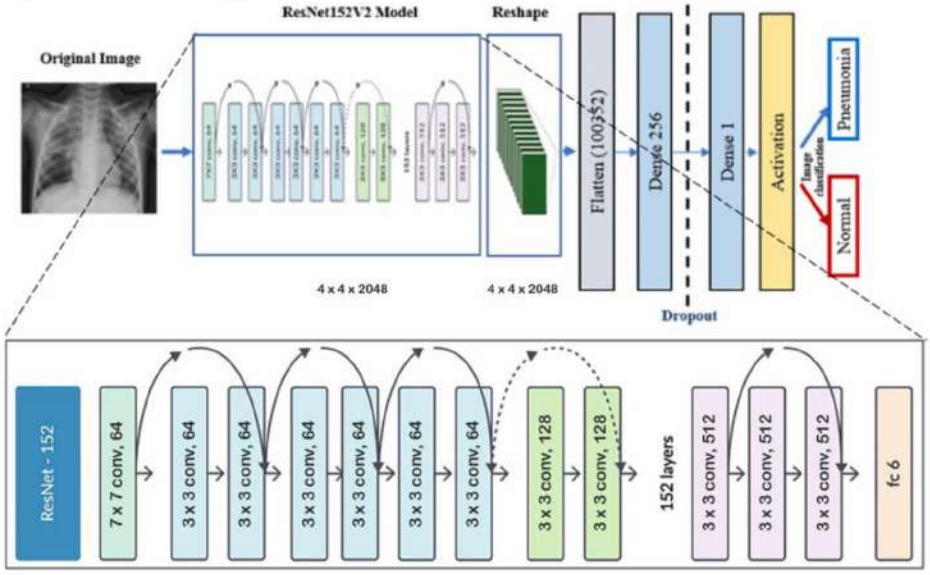


Figure 13. Layers of ResNet152.

The convolution layer constitutes the fundamental mechanism for feature extraction within the neural network. By applying a sequence of learnable filters (kernels) to the input imagery, this layer processes raw visual data to synthesize representative feature maps.

To introduce non-linearity into the network architecture, a transformation is applied to the output of each convolutional layer. The Rectified Linear Unit (ReLU) is the most widely adopted activation function due to its computational efficiency and ability to accelerate gradient convergence. Mathematically, ReLU is defined as a piecewise linear function: it outputs the input value directly if positive ($f(x) = x$), and outputs zero if negative ($f(x) = 0$). This characteristic significantly reduces training latency and often enhances overall model performance compared to alternative activation functions.

The pooling layer serves to summarize and down-sample the feature maps generated by the convolution operations. This reduction in spatial dimensionality decreases the total number of trainable parameters, thereby optimizing computational efficiency and mitigating the risk of overfitting. Two primary pooling strategies are utilized: max pooling, which extracts the maximum value within a specific window, and average pooling, which computes the arithmetic mean of the input elements.

Batch normalization is implemented to stabilize and accelerate the convergence of the network during the training phase. By normalizing the output of the preceding layer, this technique acts as a form of regularization, enabling the utilization of higher learning rates without compromising training stability.

5. | THE PROPOSED BLOCKCHAIN-BASED PHARMACEUTICAL SYSTEM

This section demonstrates the practical application of the proposed blockchain algorithm within the context of the pharmaceutical supply chain, as illustrated in Figure 14. The system architecture facilitates the secure integration of the proposed medical diagnostic kits and sensing devices, establishing a decentralized network connection that links patients directly with physicians and health authorities.

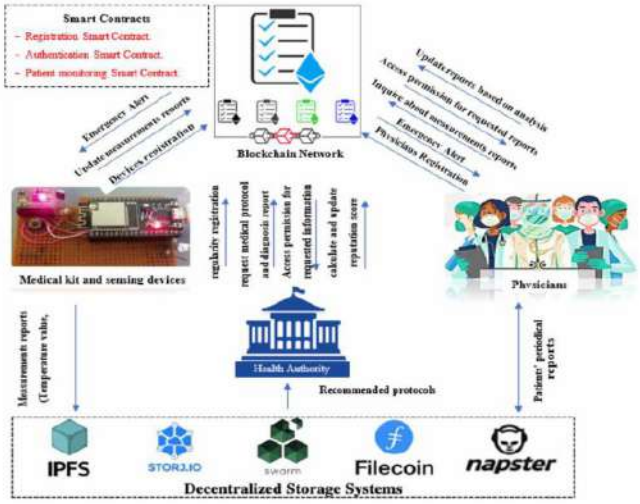


Figure 14. Proposed system architecture for blockchain implementation in the pharmaceutical supply sector.

The architectural framework of the proposed blockchain-integrated pharmaceutical supply chain establishes a secure interconnection between medical diagnostic kits, physicians, and Health Authorities. To ensure data integrity and unauthorized access prevention, the network employs a suite of specialized Smart Contracts, including:

- Registration and Authentication Contracts: For verifying network participants.

- Patient Monitoring Contracts: For automated data tracking.
- Consent Management Contracts: For handling data privacy permissions.
- Drug Prescription Verification: For validating pharmaceutical orders.

The operational dynamics of the system components are defined as follows:

1. Medical Kits and Sensing Devices : these devices form the data acquisition layer. Initially, the kit initiates a registration request to the Health Authority via the blockchain to establish a secure session with the decentralized storage system. A failed login triggers an immediate emergency alert. Upon successful authentication, the device transmits real-time physiological data—specifically Temperature, Pulse Rate, and SpO2—to physicians upon request. Furthermore, the kit is capable of committing final measurement reports directly to the decentralized storage nodes.
2. Physicians Practitioners : must first authenticate via the blockchain to access the decentralized storage repositories managed by the Health Authority. Following successful validation, physicians can query specific patient measurement reports. Access to these records requires obtaining explicit permission via the network's consent mechanisms. Once granted, physicians analyze the data and update the patient's clinical file.
3. The Health Authority Functioning : as the governance node, the Health Authority oversees all network operations initiated by physicians and medical devices. Its responsibilities include validating registration requests, dispensing appropriate medical protocols and diagnostic reports, managing information access requests, and calculating reputation scores for network participants.
4. Decentralized Storage Systems : this layer serves as the immutable repository for patient data and treatment protocols, utilizing distributed storage protocols such as IPFS, STORJ.IO, or SWARM. It accepts direct data inputs (biometric measurements) from medical kits and facilitates the retrieval and update of clinical reports by authorized physicians.

The user journey within this blockchain-based ecosystem follows a structured sequence:

1. Digital Onboarding: The patient logs into the web portal to register, submitting personal demographics and current symptoms. This initial data is utilized to generate a preliminary treatment protocol and schedule an appropriate clinical appointment. All inputs are immediately encrypted and archived in the decentralized storage.
2. Clinical Diagnostic Process: Upon visiting the clinic, the patient undergoes the two-stage diagnostic procedure (Biometric Sensing followed by conditional X-ray imaging). The sensing components (Node-MCU, SpO2, and Temperature sensors) acquire vital signs which determine the necessity of proceeding to the X-ray stage. All diagnostic outputs are appended to the patient's decentralized file, remaining accessible to authorized medical staff for real-time review.
3. Treatment Assignment: Based on the sensing element readings, a specific treatment and cure protocol is assigned and immutably recorded in the patient's file within the storage system.
4. Longitudinal Care: For subsequent visits, the system retrieves the comprehensive historical record, including prior symptoms and administered protocols, ensuring that any new symptoms are integrated into a holistic, continuous health profile.

6. | EXPERIMENTAL RESULTS

The experimental validation and subsequent analysis were conducted utilizing the Google Colaboratory (Colab) environment. This open-source, cloud-based platform facilitates the distribution of Jupyter notebooks tailored for deep learning applications. The computational infrastructure provided by Colab included an NVIDIA Tesla K80 GPU with 12 GB of RAM, supporting continuous operations for up to 12 hours. The software stack employed for these experiments incorporated standard data science and machine learning libraries, including NumPy, pandas, TensorFlow, and Matplotlib.

Optimization was achieved using the Adam optimizer, initialized with a learning rate of 0.001. To enhance model convergence, a dynamic learning rate scheduling strategy was implemented. This adaptive mechanism utilized a reduction factor of 0.5, a patience threshold of 5 epochs, and a minimum learning rate floor of 10^{-3}. Furthermore, to prevent overfitting and optimize computational resources, an early stopping protocol was enforced based on validation loss monitoring; specifically, the training process was configured to terminate if no improvement in validation loss was observed over 5 consecutive epochs. The training parameters were standardized at 20 epochs with a batch size of 64.

For the final classification output, the model employs a Sigmoid activation function at the output layer. The mathematical formulation of this activation is defined by Equation (1) and graphically represented in Figure 15.

$$\sigma(z) = \frac{1}{1+e^{-z}}. \tag{1}$$

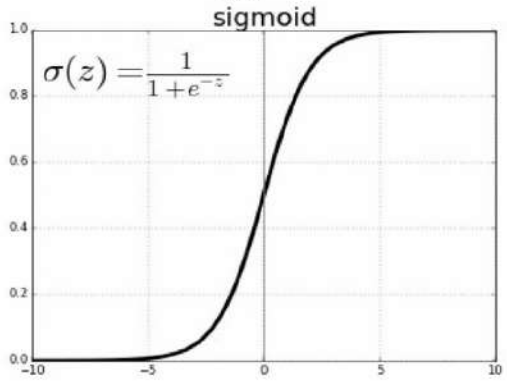


Figure 15. Sigmoid activation function in the output layer.

The subsequent sections delineate the data preprocessing pipeline, including image normalization and augmentation techniques. Data preparation is prioritized to enhance the visual quality of the input data for the training operation. This enhancement involves optimizing various parameters, such as contrast elevation, the modulation of high and low spatial frequency components, and the reduction of image noise. specifically, in this study, all input images are resized to standardized dimensions of 224 × 224 pixels. Furthermore, pixel intensity is normalized using the "min–max" technique, rescaling the original 8-bit values (0–255) to a normalized distribution. This standardization effectively eliminates bias factors, ensuring a uniform distribution across the dataset.

Figure 16 illustrates the accuracy trajectory of the ResNet152 model over the course of 20 training epochs, highlighting the peak performance values achieved. Conversely, Figure 17 depicts the loss curves for the same period. An analysis of these trends reveals a clear inverse

correlation: as the number of epochs increases, the loss values consistently diminish. The algorithm achieved its optimal accuracy at the point of minimal loss convergence.

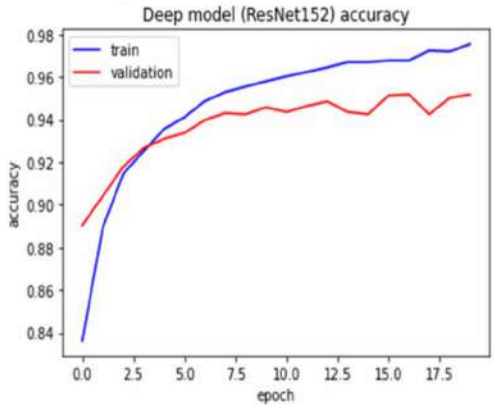


Figure 16. Accuracy curve based on 20 epochs for ResNet152.

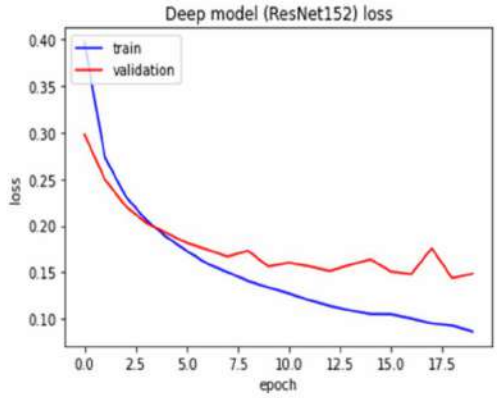


Figure 17. Losses curve based on 20 epochs for ResNet152.

The selection of the ResNet152 architecture was predicated on a comparative performance evaluation against alternative models, specifically a linear baseline and DenseNet121. The analysis demonstrated that ResNet152 consistently yielded superior accuracy compared to the other algorithms tested. To identify the optimal solution for this specific classification problem, a variety of architectures were assessed. A unifying characteristic across all tested models was the incorporation of transfer learning; each utilized a pre-trained base model supplemented by additional layers adapted to the specific domain. This methodology significantly accelerates the training process. While the underlying base architectures differed, all were fundamentally Convolutional Neural Networks (CNNs). CNNs serve as the standard architectural foundation for image classification tasks due to their inherent capability to extract hierarchical features, ranging from simple edges and lines to complex geometric shapes.

The initial experimental baseline was established using a simple linear model featuring a single trainable hidden layer, coupled with a pre-trained ResNet base where all parameters were frozen (untrainable). Subsequent iterations improved upon this by employing deep learning techniques and integrating additional hidden layers to enhance predictive performance.

Furthermore, the evaluation included DenseNet architectures, which are noted for requiring fewer parameters and facilitating feature reuse. These characteristics typically result

in more compact models that have achieved state-of-the-art performance on competitive datasets, often outperforming standard CNN or ResNet counterparts. However, in the specific context of this study, ResNet152 proved most effective. A quantitative comparison between the Linear, DenseNet121, and ResNet152 models is presented in Table 2.

Table 2. Comparison between linear, DenseNet121, and ResNet152 models.

Model	Training Accuracy	Training Loss	Validation Accuracy	Validation Loss
Linear	95.7%	13.8%	94.3%	16.4%
DenseNet121	88.5%	30.3%	87.4%	30.5%
ResNet152	97.5%	8.6%	95.2%	14.9%

Figures 18 through 21 provide a comparative illustration of the performance metrics for the Linear, DenseNet121, and ResNet152 architectures. These figures delineate the Training Accuracy (Figure 18), Validation Accuracy (Figure 19), Training Loss (Figure 20), and Validation Loss (Figure 21), respectively.

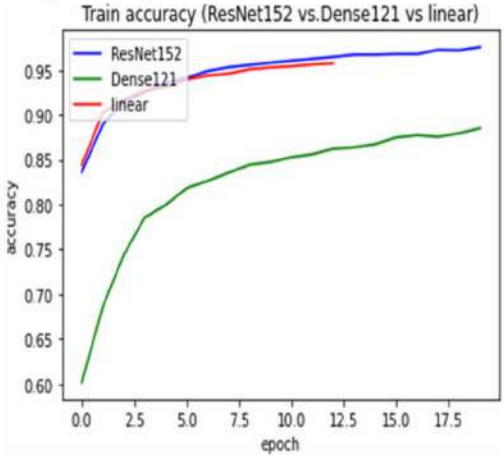


Figure 18. Training Accuracy curves for ResNet152, Dense121, and linear models.

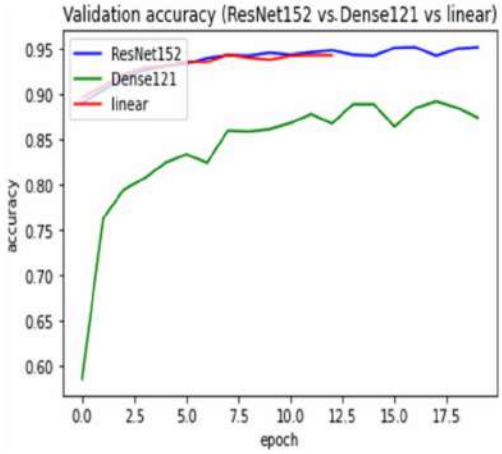


Figure 19. Validation Accuracy curves for ResNet152, Dense121, and linear models.

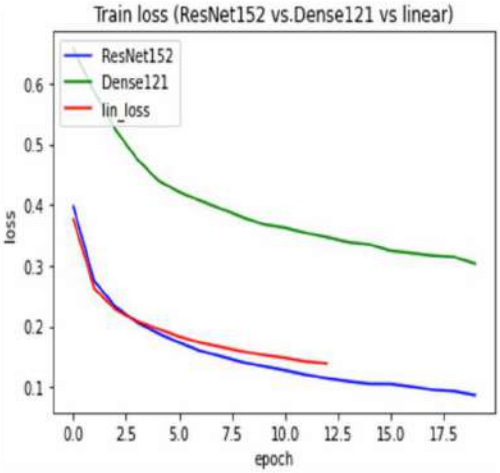


Figure 20. Training Loss curves for ResNet152, Dense121, and linear models.

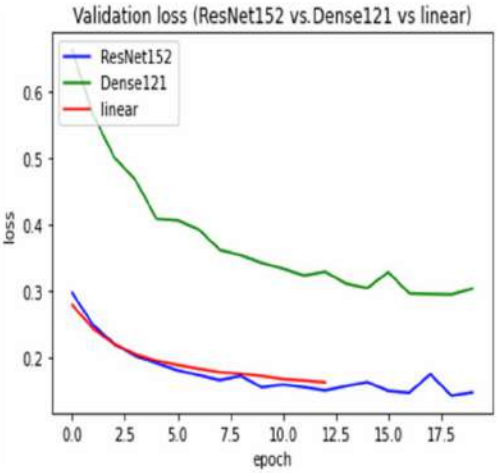


Figure 21. Validation Loss curves for ResNet152, Dense121, and linear models.

7. | RESULT DISCUSSION

As detailed in Table 2, the linear model demonstrates superior performance relative to the DenseNet121 architecture, yielding higher training and validation accuracy alongside reduced loss values. The implementation of the deep learning-based ResNet152 model marked a significant improvement over the linear baseline; training and validation accuracies reached 97.5% and 95.2%, respectively, while the corresponding loss metrics decreased to 8.6% and 14.9%.

Furthermore, the training dynamics over 20 epochs, illustrated in Figure 17 and Figure 18, confirm that the ResNet152 model consistently attains higher training and validation accuracy compared to both the DenseNet121 and linear models. Complementing this, Figure 19 and Figure 20 reveal that the ResNet152 architecture achieves significantly lower training and validation loss throughout the training duration relative to the comparative models.

8. | CONCLUSIONS

The Internet of Things (IoT) has emerged as a transformative technology across numerous sectors, with particularly significant applications in healthcare. However, IoT implementations

specifically within medical environments remain susceptible to a diverse array of security vulnerabilities and cyber-attacks. To address these critical challenges, this study designed a secure and efficient IoT-based smart healthcare ecosystem underpinned by blockchain technology. A key innovation of this system is its capacity for autonomous operation without human intervention, thereby effectively safeguarding medical personnel from exposure to infectious diseases.

Furthermore, this research proposed a robust, automated methodology for COVID-19 detection utilizing X-ray imagery. By leveraging transfer learning through the ResNet152 architecture, the system achieves high-performance automated diagnosis. The paper also introduced a novel blockchain-based framework for pharmaceutical supply chain management.

Comparative analysis against contemporary state-of-the-art algorithms demonstrates that the proposed ResNet152 model delivers superior performance quality. Over a training course of 20 epochs, the algorithm achieved significantly higher accuracy and lower loss metrics compared to alternative models, attaining a training accuracy of 97.5% and a validation accuracy of 95.2%.

Future research will focus on benchmarking the proposed system against a broader spectrum of algorithms to further validate its robustness. Additionally, plans are underway to deploy the framework within a physical hospital setting as a pilot project, with the aim of evaluating its real-world efficacy for potential large-scale generalization. Further investigation into alternative deep learning architectures will also be conducted to explore potential performance enhancements.

REFERENCES

We use the standard APA (American Psychological Association) style in compiling bibliography. Writing a bibliography uses alphabetical order and with numbering. The same author (with different works) must have his full name written instead of using a dash. Examples of writing you can see below:

1. Islam, S.; Islam, T.; Islam, M.R. New coronavirus variants are creating more challenges to global healthcare system: A brief report on the current knowledge. Clin. Pathol. 2022, 15, 2632010X221075584.
2. Chemali, S.; Mari-Sáez, A.; El Bcheraoui, C.; Weishaar, H. Health care workers' experiences during the COVID-19 pandemic: A scoping review. Hum. Resour. Health 2022, 20, 27.
3. World Health Organization. The Impact of COVID-19 on Health and Care Workers: A Closer Look at Deaths. World Health Organization. 2021. Available online: https://apps.who.int/iris/handle/10665/345300 (accessed on 17 March 2022).
4. Salih, K.O.M.; Rashid, T.A.; Radovanovic, D.; Bacanin, N. A comprehensive survey on the Internet of Things with the industrial marketplace. Sensors 2022, 22, 730.

5. Zhang, C.; Zhu, L.; Xu, C.; Lu, R. PPDP: An efficient and privacy-preserving disease prediction scheme in cloud-based e-healthcare system. Future Gener. Comput. Syst. 2018, 79, 16–25.
6. Ali, H.M.; Liu, J.; Bukhari SA, C.; Rauf, H.T. Planning a secure and reliable IoT-enabled FOG-assisted computing infrastructure for healthcare. Clust. Comput. 2021, 25, 2143–2161.
7. Kumar, P.M.; Hong, C.S.; Afghah, F.; Manogaran, G.; Yu, K.; Hua, Q.; Gao, J. Clouds proportionate medical data stream analytics for internet of things-based healthcare systems. IEEE J. Biomed. Health Inform. 2021, 26, 973–982.
8. Namasudra, S. Fast and secure data accessing by using DNA computing for the cloud environment. IEEE Trans. Serv. Comput. 2020, 15, 2289–2300.
9. Namasudra, S.; Deka, G.C.; Johri, P.; Hosseinpour, M.; Gandomi, A.H. The revolution of blockchain: State-of-the-art and research challenges. Arch. Comput. Methods Eng. 2020, 28, 1497–1515.
10. Sharma, P.; Moparthi, N.; Namasudra, S.; Shanmuganathan, V.; Hsu, C. Blockchain-based IoT architecture to secure healthcare system using identity-based encryption. Expert Syst. 2020, 39, e12915.
11. Liang, X.; Shetty, S.; Tosh, D.; Kamhoua, C.; Kwiat, K.; Njilla, L. Provchain: A Blockchain-Based Data Provenance Architecture in Cloud Environment with Enhanced Privacy and Availability. In Proceedings of the 2017 17th IEEE/ACM International Symposium on Cluster, Cloud and Grid Computing (CCGRID), Madrid, Spain, 14–17 May 2017; pp. 468–477.
12. Kish, L.J.; Topol, E.J. Unpatients—Why patients should own their medical data. Nat. Biotechnol. 2015, 33, 921.
13. Tariq, N.; Qamar, A.; Asim, M.; Khan, F. Blockchain and Smart Healthcare Security: A Survey. The 6th International Workshop on Cyber Security and Digital Investigation (CSDI). Procedia Comput. Sci. 2020, 175, 615–620.
14. Ali, A.; Khan, F.A. A broadcast-based key agreement scheme using set reconciliation for wireless body area networks. J. Med. Syst. 2014, 38, 33.
15. Khan, F.A.; Gumaei, A.; Derhab, A.; Hussain, A. A novel two-stage deep learning model for efficient network intrusion detection. IEEE Access 2019, 7, 30373.
16. Tariq, N.; Khan, F.A. Match the Sound Captcha. In Information Technology-New Generations; Springer: Berlin/Heidelberg, Germany, 2018; pp. 803–808.
17. Liang, X.; Zhao, J.; Shetty, S.; Liu, J.; Li, D. Integrating blockchain for data sharing and collaboration in mobile healthcare applications. In Proceedings of the 2017 IEEE 28th Annual International Symposium on Personal, Indoor, and Mobile Radio Communications (PIMRC), Montreal, QC, Canada, 8–13 October 2017; pp. 1–5.
18. Khalid, U.; Asim, M.; Baker, T.; Hung, P.C.; Tariq, M.A.; Rafferty, L. Adecentralized lightweight blockchain-based authentication mechanism for iot systems. Clust. Comput. 2020, 23, 2067–2087.
19. Linn, L.A.; Koo, M.B. Blockchain for Healthdata and Its Potential Use in Health IT and Healthcare Related Research. In Proceedings of the ONC/NIST Use of Blockchain for Healthcare and Research Workshop, Gaithersburg, MA, USA, 26–27 September 2016.
20. Hardin, T.; Kotz, D. Blockchain in Health Data Systems: A Survey. In Proceedings of the 2019 Sixth International Conference on Internet of Things: Systems, Management and Security (IOTSMS), Granada, Spain, 22–25 October 2019; pp. 490–497.

21. Yaqoob, I.; Salah, K.; Jayaraman, R.; Al-Hammadi, Y. Blockchain for healthcare data management: Opportunities, challenges, and future recommendations. Neural Comput. Appl. 2021, 34, 11475–11490.
22. Nakamoto, S. Bitcoin: A Peer-To-Peer Electronic Cash System. 2008. Available online: https://bitcoin.org/bitcoin.pdf (accessed on 15 June 2020).
23. Dinh, T.T.A.; Liu, R.; Zhang, M.; Chen, G.; Ooi, B.C.; Wang, J. Untangling blockchain: A data processing view of block chain systems. IEEE Trans. Knowl. Data Eng. 2018, 30, 1366.
24. Pallivalappil, A.S.; Ahmad, S.S.; Raju, Y.; Kumar, C.K.; Krishnaiah, N. Applications of Ensuring Security and Privacy Using Block Chain with IoT for Health Record. In Proceedings of the 2nd International Conference on Advance Computing and Innovative Technologies in Engineering (ICACITE), Greater Noida, India, 28–29 April 2022; pp. 1911–1917.
25. Shi, S.; He, D.; Li, L.; Kumar, N.; Khan, M.K.; Choo, K.K.R. Applications of Blockchain in Ensuring the Security and Privacy of Electronic Health Record Systems: A Survey. Comput. Secur. 2020, 97, 101966.
26. Gordon, W.J.; Catalini, C. Blockchain Technology for Healthcare: Facilitating the Transition to Patient-Driven Interoperability. Comput. Struct. Biotechnol. J. 2018, 16, 224–230.
27. Nguyen, D.C.; Pathirana, P.N.; Ding, M.; Seneviratne, A. E-Healthcare System Using Blockchain for Secure EHRs Sharing of Mobile Cloud Based with Machine Learning. Int. J. Sci. Dev. Res. 2020, 5, 66792–66806.
28. Solomon, D.H.; Rudin, R.S. Digital health technologies: Opportunities and challenges in rheumatology. Nat. Rev. Rheumatol. 2020, 16, 525–535.
29. Gianfrancesco, M.A.; Goldstein, N.D. A narrative review on the validity of electronic health record-based research in epidemiology. BMC Med. Res. Methodol. 2021, 21, 234.
30. Kim, E.; Rubinstein, S.M.; Nead, K.T.; Wojcieszynski, A.P.; Gabriel, P.E.; Warner, J.L. The Evolving Use of Electronic Health Records (EHR) for Research. In Seminars in Radiation Oncology; WB Saunders: Philadelphia, PA, USA, 2019; Volume 29, pp. 354–361.
31. Ahmad, R.W.; Salah, K.; Jayaraman, R.; Yaqoob, I.; Ellahham, S.; Omar, M. The role of blockchain technology in telehealth and telemedicine. Int. J. Med. Inform. 2021, 148, 104399.
32. Kassab, M.; DeFranco, J.; Malas, T.; Neto VV, G.; Destefanis, G. Blockchain: A panacea for electronic health records? In Proceedings of the 2019 IEEE/ACM 1st International Workshop on Software Engineering for Healthcare (SEH), 2019, Montreal, QC, Canada, 27 May 2019; pp. 21–24.
33. Fang, H.S.A.; Tan, T.H.; Tan, Y.F.C.; Tan, C.J.M. Blockchain personal health records: Systematic review. J. Med. Internet Res. 2021, 23, e25094.
34. Katal, A.; Sethi, V.; Choudhury, T. Potential of Blockchain in Telemedicine. In Telemedicine: The Computer Transformation of Healthcare; Springer: Cham, Switzerland, 2022; pp. 167–184.
35. Mohammed, M.N.; Desyansah, S.F.; Al-Zubaidi, S.; Yusuf, E. An internet of things-based smart homes and healthcare monitoring and management system. J. Phys. Conf. Ser. 2020, 1450, 012079.

36. Cernian, A.; Tiganoaia, B.; Sacala, I.; Pavel, A.; Iftemi, A. PatientDataChain: A blockchain-based approach to integrate personal health records. Sensors 2020, 20, 6538.
37. Radiopaedia Web Page. Available online: https://radiopaedia.org/ (accessed on 1 August 2022).
38. SIRM Web Page. Available online: https://sirm.org/en/ (accessed on 1 August 2022).
39. EURORAD Web Page. Available online: https://www.eurorad.org/ (accessed on 1 August 2022).